Elastic and inelastic electron scattering from ^{50,52,54}Cr

J. W. Lightbody, Jr.,* J. B. Bellicard, J. M. Cavedon, B. Frois, D. Goutte,
M. Huet, Ph. Leconte, A. Nakada, Phan Xuan Ho, S. K. Platchkov, and S. Turck-Chieze
Département de Physique Nucléaire, Centre d'Etudes Nucléaires de Saclay, 91190 Gif-sur-Yvette Cedex, France

C. W. de Jager, J. J. Lapikás, and P. K. A. de Witt Huberts
Nationaal Instituut voor Kernfysica en Hoge-Energiefysica, 1009 AJ Amsterdam, The Netherlands
(Received 28 June 1982)

Elastic and inelastic electron scattering cross sections are given for ^{50,52,54}Cr at momentum transfers between 0.15 and 2.6 fm^{-1}. Ground state charge distributions are derived from a combined analysis of these data and muonic atom data. Deduced values of the rms charge radii are given. Comparison is made between the experimental charge distributions and density dependent Hartree-Fock-Bogolyubov calculations. Inelastic scattering form factors for 2^+, 4^+, and 6^+ states up to 4 MeV excitation are given along with shell model and phenomenological model fits to those data, $B(EL)$ values, multipole dependence of effective charges, and other model parameters.

[NUCLEAR REACTIONS ^{50,52,54}Cr(e,e'), E=30–400 MeV. Measured $\sigma(E,\theta)$. Deduced ground state charge distributions compared to Hartree-Fock. Deduced inelastic form factors compared to shell model.]

I. INTRODUCTION

Our interest in the even isotopes ^{50,52,54}Cr arises from the considerable theoretical effort invested in the study of level schemes and transition probabilities for f-shell nuclei.[1] We report here the results of an elastic and inelastic electron scattering experiment on the above isotopes. The inelastic studies were carried out to an excitation energy of 4 MeV and extend to the low lying 2^+, 4^+, and 6^+ states because these states are expected to be only modestly impure shell model configurations and therefore calculable. We investigate whether calculations based on the seniority scheme, which consider only $f_{7/2}$ recoupling configurations with mixing of seniority 2 and 4, are adequate to describe the data, or whether contributions from more complicated configurations such as $1f \rightarrow 2p$ are required. Furthermore, enhancement of transition strengths over shell model estimates depends strongly on the proximity of configurations which can mix with the dominant $f_{7/2}$ amplitude to achieve the desired angular momentum. We therefore expect this enhancement to be a strong function of the transition multipolarity. Because of the broad momentum transfer range of the inelastic scattering data ($0.9 \leq q \leq 2.6$ fm^{-1}) we are able to assess theory in more detail than would be possible with low momentum transfer experiments, radiative decay experiments, or by comparison of experimental and theoretical level energies. The elastic scattering work was carried out with a view towards understanding changes in the charge distributions near a shell closure, in this case, the neutron $f_{7/2}$ shell. There are μ-mesic x-ray data[2] which indicate a shrinkage in the root mean square (rms) radius of ^{52}Cr with respect to ^{50}Cr and ^{54}Cr. Hartree-Fock-Bogolyubov calculations[3] of the charge distributions for ^{50,52,54}Cr using density-dependent effective forces indicate differences in the rms radii of isotope pairs (52–50 and 54–52) which are significantly less than observed in the μ-mesic x-ray work. Also, there is some indication[4] that there is a softness in these nuclei with respect to deformation. The static quadrupole moments of the first 2^+ states make a transition from oblate to near spherical and back to oblate in going from ^{50}Cr to ^{54}Cr. Detailed mapping of the ground state and transition charge distributions may help in understanding these phenomena.

II. EXPERIMENTAL EQUIPMENT AND METHODS

The experiment was carried out at the 600 MeV Saclay Accelerateur Lineaire de Saclay (ALS) linac and at the 90 MeV NIKHEF [formerly Instituut

voor Kernphysisch Onderzoek (IKO)] linac. All of the inelastic data and the elastic data above $q=0.8$ fm^{-1} were taken at the Saclay ALS using the 900 MeV/c magnetic spectrometer with a 512-channel multiwire proportional counter focal plane array.[5] The beam current at both Saclay ALS and NIKHEF was monitored with a torroidal ferrite core transformer, Faraday cup, and electronic integrator. Isotopically enriched Cr-oxide target material was obtained from Oak Ridge National Laboratory and electrolytically reduced to metal foil targets of 20 to 40 mg/cm^2. The targets had isotopic purities of greater than 99% for the ^{52}Cr target, 91.68% for the ^{50}Cr target, and 97.2% for the ^{54}Cr target. Elastic scattering data were taken at 200 and 400 MeV at the Saclay ALS ($0.8 \leq q \leq 2.6$ fm^{-1}), and at NIKHEF between 30 and 85 MeV ($0.15 \leq q \leq 0.84$ fm^{-1}). There was a sufficient overlap in the q range of data taken at the different laboratories to ensure consistent normalizations of the different data sets (Saclay ALS and NIKHEF). The inelastic data were taken only at the Saclay ALS, with an incident beam energy of 398.2 MeV, and for scattering angles between 25° and 80°. The overall momentum resolution for the Saclay ALS part of the experiment was 4×10^{-4}, permitting relatively clean extraction of cross sections. For this experiment the targets were oriented in transmission mode. The incident beam energy was determined to ±0.05% at the Saclay ALS and ±0.15% at NIKHEF. Scattering angles were determined to ±0.05° and ±0.08° at the Saclay ALS and NIKHEF, respectively.

III. RESULTS—ELASTIC SCATTERING

The measured elastic scattering cross sections are given in Tables I–III. The NIKHEF data result from measurements of the ^{50,52,54}Cr elastic scatter-

TABLE I. ^{50}Cr elastic scattering cross sections (mb). We use the following notation for uncertainties: 0.000(1)−2 corresponds to $0.000\times10^{-2}\pm0.001\times10^{-2}$.

E (MeV)	θ (deg)	σ	($\delta\sigma$)	$\Delta\theta$ (deg)	$\Delta\phi$ (deg)	E (MeV)	θ (deg)	σ	($\delta\sigma$)	$\Delta\theta$ (deg)	$\Delta\phi$ (deg)
30	60	0.4270	(28)+2	±0.0	±0.0	200	65	0.1049	(30)−2	±0.9	±2.9
35		0.2964	(20)+2				70	0.1012	(33)−2		
40		0.2165	(20)+2				75	0.875	(30)−3		
45		0.1608	(13)+2				80	0.587	(19)−3		
50		0.1208	(10)+2				85.06	0.358	(12)−3		
55		0.9271	(70)+1				90	0.1909	(79)−3		
60		0.7089	(50)+1				95	0.871	(37)−4		
65		0.5578	(42)+1				38	0.658	(16)+0	±0.3	±0.3
70		0.4355	(33)+1								
75		0.3382	(25)+1			401.6	35	0.419	(18)−2	±0.9	±2.7
80		0.2702	(23)+1				40	0.2042	(89)−2		
85		0.2121	(17)+1				60	0.745	(49)−5		
30	120	0.1296	(09)+1				62.4	0.654	(29)−5		
35		0.8258	(70)+0				67.5	0.267	(18)−5		
40		0.5284	(42)+0				72.5	0.808	(55)−6	±1.0	±4.0
45		0.3462	(29)+0								
50		0.2215	(16)+0			398.2	35	0.453	(20)−2	±0.9	±2.7
55		0.1431	(14)+0				37.5	0.322	(14)−2	±1.08	±4.0
60		0.9039	(81)−1				40	0.2095	(92)−2		
65		0.5685	(48)−1				42.5	0.1044	(45)−2		
70		0.3455	(30)−1				45	0.448	(20)−3		
75		0.2062	(19)−1				47.5	0.1777	(78)−3		
80		0.1188	(10)−1				52.5	0.1046	(45)−4		
85		0.6472	(54)−2				55	0.487	(22)−5		
							57.5	0.669	(29)−5		
200	35	0.1324	(24)+1	±0.3	±0.3		60	0.830	(37)−5		
	38.05	0.656	(17)+0				62.5	0.647	(29)−5		
	41	0.3043	(80)+0				65	0.540	(24)−5		
	45	0.1122	(29)+0				70	0.1755	(78)−5		
	50	0.2757	(69)−1	±0.4	±1.15		75	0.444	(76)−6		
	55	0.588	(17)−2				80	0.67	(25)−7		
	60	0.1551	(43)−2	±0.4	±4.0						

TABLE II. ^{52}Cr elastic scattering cross sections (mb). We use the following notation for uncertainties: 0.000(1)−2 corresponds to $0.000\times10^{-2}\pm0.001\times10^{-2}$.

E (MeV)	θ (deg)	σ	$(\delta\sigma)$	$\Delta\theta$ (deg)	$\Delta\phi$ (deg)
30	60	0.4260	(37)+2	±0.0	±0.0
35		0.2996	(27)+2		
40		0.2175	(20)+2		
45		0.1612	(16)+2		
50		0.1219	(11)+2		
55		0.9297	(85)+1		
60		0.7199	(72)+1		
65		0.5574	(56)+1		
70		0.4380	(42)+1		
75		0.3402	(30)+1		
80		0.2716	(30)+1		
85		0.2136	(21)+1		
30	120	0.1289	(11)+1		
35		0.8246	(87)+0		
40		0.5287	(52)+0		
45		0.3500	(35)+0		
50		0.2253	(26)+0		
55		0.1461	(15)+0		
60		0.9225	(98)−1		
65		0.5792	(56)−1		
70		0.3515	(39)−1		
75		0.2118	(22)−1		
80		0.1202	(11)−1		
85		0.6639	(76)−2		
200	35	0.1317	(21)+1	±0.3	±0.3
	38.05	0.662	(14)+0		
	41	0.3187	(69)+0		
	45	0.1188	(28)+0		
	50	0.2809	(64)−1	±0.4	±1.15
	55	0.608	(14)−2		
	60	0.1588	(39)−2	±0.4	±4.0
	65	0.1160	(32)−2	±0.9	±2.9
	70	0.1177	(31)−2		
	75	0.985	(29)−3		
	80	0.654	(20)−3		
	85.06	0.442	(14)−3		
	90	0.2076	(69)−3		
	95	0.1133	(44)−3		
	38	0.666	(16)+0	±0.3	±0.3
401.6	35	0.466	(13)−2	±0.9	±2.7
	40	0.2302	(94)−2		
	47.5	0.1784	(70)−3	±1.0	±4.0
	60	0.948	(47)−5	±0.9	±2.7
	62.5	0.880	(34)−5		
	67.5	0.468	(19)−5	±1.0	±4.0
	72.5	0.1188	(71)−5		
	77.5	0.228	(23)−6		
398.2	35	0.540	(21)−2	±0.9	±2.7
	37.5	0.384	(15)−2	±1.08	±4.0
	40	0.2395	(94)−2		
	42.5	0.1248	(49)−2		
	47.5	0.2000	(79)−3		
	50	0.521	(21)−4		
	52.5	0.1154	(43)−5		
	55	0.643	(26)−5		
	57.5	0.912	(36)−5		
	60	0.1084	(43)−4		
	62.5	0.976	(39)−5		
	65	0.726	(30)−5		
	70	0.2439	(96)−5		
	75	0.720	(75)−6		
	80	0.72	(12)−7		

ing cross sections relative to ^{12}C, which were normalized to the recent analysis by Cardman *et al.*[6] of the combined NIKHEF, Stanford, and National Bureau of Standards (NBS) elastic electron scattering data for ^{12}C. The total uncertainties for the NIKHEF Cr data were obtained by adding the statistical part in quadrature with one half percent estimated systematic uncertainty. This latter part of the uncertainty is an estimate based on uncertainty in the ^{12}C reference cross sections and possible target nonuniformity and/or other instrumental effects. The Saclay ALS 200, 398.2, and 401.6 MeV data are absolute measurements, not referenced to ^{12}C. The efficiency of the counter system was established by measuring the ^{12}C cross section at low momentum transfer. In the Saclay ALS 200 MeV data, uncertainties were obtained by adding the statistical part in quadrature with 2% estimated systematic uncertainty. Similarly, uncertainties in the 398.2 and 401.6 MeV data sets were formed from a statistical part and a 4% estimated systematic uncertainty. Some of this uncertainty may come from inhomogeneities in the targets. All of these data have been adjusted to remove effects of the presence of other isotopes. The angles $\Delta\theta$ and $\Delta\phi$ (Tables I–III) are the spectrometer azimuthal and polar acceptance angles. We have used a Fourier-Bessel expansion method[7] for the ground state charge distribution to fit the present data. The calculated cross sections needed in the fitting procedure were obtained with the partial wave code HEINEL.[8] The fitting procedure includes the effect of convoluting the true angular dependence of the cross sections with the finite spectrometer acceptance (both horizontal and

TABLE III. ^{54}Cr elastic scattering cross sections (mb). We use the following notation for uncertainties: 0.000(1)−2 corresponds to $0.000\times10^{-2}\pm0.001\times10^{-2}$.

E (MeV)	θ (deg)	σ	$(\delta\sigma)$	$\Delta\theta$ (deg)	$\Delta\phi$ (deg)	E (MeV)	θ (deg)	σ	$(\delta\sigma)$	$\Delta\theta$ (deg)	$\Delta\phi$ (deg)
30	60	0.4268	(30)+2	±0.0	±0.0		65	0.1125	(33)−2	±0.9	±2.9
35		0.2965	(23)+2				70	0.1078	(31)−2		
40		0.2154	(16)+2				75	0.933	(29)−3		
45		0.1599	(13)+2				80	0.602	(18)−3		
50		0.1205	(09)+2				85.06	0.345	(12)−3		
55		0.9193	(76)+1				90	0.1939	(70)−3		
60		0.7055	(57)+1				95	0.856	(34)−4		
65		0.5507	(44)+1				38	0.612	(14)−4	±0.3	±0.3
70		0.4296	(35)+1								
75		0.3337	(25)+1			401.6	35	0.422	(17)−2	±0.9	±2.7
80		0.2666	(20)+1				40	0.1991	(83)−2		
85		0.2082	(16)+1				47.5	0.1413	(59)−3	±1.0	±4.0
30	120	0.1297	(09)+1				60	0.866	(36)−5	±0.9	±2.7
35		0.8156	(72)+0				62.4	0.670	(28)−5		
40		0.5215	(39)+0				67.5	0.2699	(96)−5	±1.0	±4.0
45		0.3428	(29)+0				72.5	0.708	(52)−6		
50		0.2160	(19)+0				77.4	0.41	(13)−7		
55		0.1404	(14)+0								
60		0.8759	(82)−1			398.2	35	0.487	(20)−2	±0.9	±2.7
65		0.5462	(46)−1				37.5	0.338	(13)−2	±1.08	±4.0
70		0.3286	(32)−1				40	0.2200	(91)−2		
75		0.1960	(20)−1				42.5	0.1039	(43)−2		
80		0.1100	(09)−1				47.5	0.1541	(63)−3		
85		0.5968	(50)−2				52.5	0.895	(37)−5		
							55	0.569	(23)−5		
200	35	0.1275	(28)+1	±0.3	±0.3		57.5	0.750	(31)−5		
	38.05	0.606	(15)+0				60	0.981	(41)−5		
	41	0.2981	(72)+0				62.5	0.700	(29)−5		
	45	0.1040	(26)+0				65	0.504	(21)−5		
	50	0.2524	(64)−1	±0.4	±1.15		70	0.1554	(63)−5		
	55	0.523	(13)−2				75	0.360	(38)−6		
	60	0.1458	(37)−2	±0.4	±4.0		80	0.31	(15)−7		

vertical). For the Saclay ALS data, we did not take into account the effect of folding in multiple scattering in the target. We found this to be of negligible importance. The NIKHEF data have been corrected for the effects of multiple scattering in the target and for finite solid angle and, therefore, represent measurements taken with zero solid angle ($\Delta\theta=\Delta\phi=0$) and zero target thickness. For computational ease in the fitting procedure we converted the NIKHEF data to an angular distribution at one energy. The scattering angles for the converted angular distribution were adjusted such that the effective momentum transfers were equal to those for the actual data. (Effective momentum transfer is defined as

$$q_{\text{effective}}=q\left[1+\frac{3Z\alpha}{2kR_{eq}}\right],$$

where R_{eq} is the radius of the uniformly charged sphere which yields the measured rms radius.) The conversion factors were iterated several times in order to be consistent with the final resultant charge distribution. The data sets for the different energies were allowed free normalization factors which were determined in a fit to the combined data. The experimental data points given in Tables I–III result from dividing measured data points by the normalizations obtained in the fit. The normalization (N) is defined by the relation

$$N=\sigma\ (\text{measured})/\sigma\ (\text{best fit})\ .$$

The form of the ground state charge distribution is assumed to be a Fourier-Bessel expansion

$$\rho(r)=\sum_{\nu=1}^{\nu_{\max}} a_\nu j_0(q_\nu r),\quad r\le R$$
$$=0,\quad r>R$$

with a normalization defined by

$$4\pi \int \rho(r) r^2 dr = 1$$

and where the q_ν are chosen such that $q_\nu R = \nu\pi$. The number of terms in the above expansion is determined by the maximum momentum transfer in the experiment ($q_{\max}$). In principle one can extract a nuclear charge distribution from (e,e) data given measurements over all momentum transfers. In practice one must deal with data over a finite q range and therefore must resort to a model of the nuclear charge distribution with a finite number of degrees of freedom. Although the present data are restricted to $q_{\max} \leq 2.6$ fm^{-1}, one expects on physical grounds that over a q range far beyond $q_{\max}$ the form factor data will be contained within an exponentially decreasing envelope. (See Borysowicz and Hetherington[9] and Dreher *et al.*[7] for further discussion.) To rule out nonphysical variations of the predicted form factors (i.e., which exceed the exponential envelope) above $q_{\max}$ and following Borysowicz and Hetherington we have appended pseudodata in the form of upper limits to our measured data, extending these upper limits out to $q=4$ fm^{-1}. These pseudodata were derived by considering the envelope of all data to be given by the expression

$$F^2(q) = Ae^{-aq} ,$$

where the constants (A) and (a) were fixed by a fit to the diffraction maxima of the actual data. The pseudodata were chosen as half of the envelope values with 100% uncertainties. We did not make a random selection of q values for these pseudodata, but rather chose pseudodata at 5° intervals from 85° to 145°, corresponding to a q range of from 2.73 to 3.87 fm^{-1}. In addition to (e,e) data for these isotopes, there exist muonic atom data of Wohlfahrt *et al.*[2] These latter data represent measurement of the $2p_{1/2}$-$1s_{1/2}$ muonic x-ray transition energies in ^{50,52,54}Cr. From these transition energies one derives generalized Barrett moments[2] of the nuclear charge distribution, defined as

$$B_K \equiv \int \rho(r) r^k e^{-\alpha' r} 4\pi r^2 dr ,$$

and an equivalent nuclear charge radius (R_k) for a uniform density spherical drop model of the nucleus, where R_k is defined such that

$$B_k = 3R_k{}^{-3} \int_0^{R_k} r^k e^{-\alpha' r} r^2 dr .$$

We have taken the Wohlfahrt *et al.* values[2] for R_k with the appropriate uncertainties, and converted them to generalized moments. These moments were then used in a combined analysis of (e,e') and muonic data by the method of iterative, nonlinear, least squares fitting. All the muonic results are summarized in Table IV.

The largest uncertainty in the muonic data results from uncertainty in the nuclear polarization (NP) correction to the absolute transition energy. We have adopted a ±40% uncertainty in this correction.[10] As can be seen in Table IV, the resultant uncertainty in the generalized moment is many times the statistical uncertainty.

Since we have data for a series of isotopes of chromium, we have analyzed the data in two ways. First, one isotope at a time, obtaining details of $\rho(r)$, and second, combined in pairs in order to extract the difference in the charge distributions between isotopes. The statistical precision of the ratios between (e,e) data for different isotope pairs is better than the absolute cross section data because of the absence of many systematic effects. In Table V we give NIKHEF data for the relative cross sections for ^{52}Cr/^{50}Cr, ^{54}Cr/^{52}Cr, and ^{54}Cr/^{50}Cr with uncertainties. The relative cross sections for all the Saclay ALS data were estimated to be no better than simply computing the ratio and uncertainties from results given in Tables I–III, and were so derived. We do not present these latter data separately. The differences in generalized Barrett moments for the several pairs of isotopes considered are much better determined than the absolute moments, due to the fact that the nuclear polarization corrections tend to cancel. For the present fits we have assumed that uncertainties in the differences in moments are deter-

TABLE IV. Summary—muonic x-ray results.

	R_k (fm)	$\pm\delta R_k^{\text{random}}$	δR_k^{NP}	$\delta R_k^{\text{total}}$	B_k (fm^k)	$\pm\delta B_k^{\text{random}}$	δB_k^{NP}	$\delta B_k^{\text{total}}$
^{50}Cr	4.6947	0.0005	0.0036	0.0041	11.698	0.002	0.017	0.019
^{52}Cr	4.6698	0.0004	0.0033	0.0037	11.584	0.002	0.015	0.017
^{54}Cr	4.7278	0.0005	0.0036	0.0041	11.850	0.002	0.017	0.019
	ΔR_k (fm)	$\pm\delta(\Delta R_k)^{\text{random}}$	$\delta(\Delta R_k)^{\text{NP}}$	$\delta(\Delta R_k)^{\text{total}}$	ΔB_k (fm^k)	$\pm\delta(\Delta B_k)^{\text{random}}$	$\delta(\Delta B_k)^{\text{NP}}$	$\delta(\Delta B_k)^{\text{total}}$
$^{52-50}$Cr	−0.0249	0.0006		0.0006	−0.1138	0.0029		0.0029
$^{54-52}$Cr	0.0580	0.0006		0.0006	0.2658	0.0029		0.0029
$^{54-50}$Cr	0.0331	0.0007		0.0007	0.1520	0.0033		0.0033

TABLE V. Elastic scattering cross section ratios (R). We use the following notation for uncertainties: $0.000(1)-2$ corresponds to $0.000\times10^{-2}\pm0.001\times10^{-2}$.

E (MeV)	θ (deg)	$R(52/50)\pm(\delta R)$		$R(54/52)\pm(\delta R)$		$R(54/50)\pm(\delta R)$	
30	60	0.9977	(53)	1.0019	(58)	0.9995	(31)
35		1.0108	(57)	0.9896	(55)	1.0003	(30)
40		1.0046	(88)	0.9903	(59)	0.9949	(54)
45		1.0025	(61)	0.9919	(58)	0.9944	(35)
50		1.0091	(67)	0.9885	(56)	0.9975	(40)
55		1.0028	(64)	0.9888	(70)	0.9916	(44)
60		1.0155	(75)	0.9800	(73)	0.9952	(44)
65		0.9993	(68)	0.9880	(63)	0.9873	(39)
70		1.0057	(70)	0.9808	(73)	0.9864	(46)
75		1.0059	(64)	0.9809	(60)	0.9867	(36)
80		1.0052	(95)	0.9816	(78)	0.9867	(46)
85		1.0071	(72)	0.9747	(64)	0.9816	(41)
30	120	0.9946	(56)	1.0062	(58)	1.0008	(40)
35		0.9985	(64)	0.9891	(67)	0.9876	(38)
40		1.0006	(76)	0.9864	(67)	0.9869	(42)
45		1.0110	(72)	0.9794	(68)	0.9902	(35)
50		1.0172	(55)	0.9587	(57)	0.9752	(37)
55		1.0210	(59)	0.9610	(54)	0.9811	(37)
60		1.0206	(75)	0.9495	(70)	0.9690	(50)
65		1.0188	(71)	0.9430	(56)	0.9608	(41)
70		1.0174	(85)	0.9348	(84)	0.9511	(53)
75		1.0272	(68)	0.9254	(57)	0.9505	(38)
80		1.0118	(74)	0.9151	(60)	0.9259	(41)
85		1.0258	(88)	0.8989	(74)	0.9221	(35)

mined purely by the statistical precision of the measurements.

The actual fitting routines are derived by minimizing

$$\chi^2=\omega_B(B^{\exp}-B^{\text{th}})^2 + \sum_{(e,e')}\omega_i(y_i-N_k\sigma_i)^2 ,$$

where $\omega_{i,B}$ are the weight factors [(uncertainty)$^{-2}$], y_i are measured (e,e) cross sections, $B^{\exp}$ is the measured generalized Barrett moment, N_k are the normalization factors for the different data sets, σ_i are the theoretical (e,e) cross sections, and B^{th} is the theoretical generalized Barrett moment. We proceed by expanding σ_i and B^{th} about some initial set of charge distribution parameters $a_\nu^{(0)}$ (derived from a three parameter Fermi model):

$$\sigma_i=\sigma_i^{(0)}+\sum_{\nu=1}^{\nu_{\max}}\frac{\partial\sigma}{\partial a_\nu}\Delta a_\nu ,$$

$$B^{\text{th}}=B^0+\sum_{\nu=1}^{\nu_{\max}}\frac{\partial B}{\partial a_\nu}\Delta a_\nu ,$$

and then solving for the Δa_ν's using matrix inversion techniques. By iteration we refine the initial starting parameters until there is no change in the values of a_ν within the desired accuracy. In the fitting of ratio data we proceed in essentially the same fashion. The observables which we are now attempting to fit become the cross section ratios σ_{A+2}/σ_A and the difference in Barrett moment for the isotope pair

$$(B_k[A+2]-B_k[A]) .$$

The above expansions become

$$\frac{\sigma_{A+2}}{\sigma_A}-1=\sum_{\nu=1}^{\nu_{\max}}\frac{1}{\sigma_A}\frac{\partial\sigma_A}{\partial a_\nu}\Delta a_\nu$$

and

$$B_k[A+2]-B_k[A]=\sum_{\nu=1}^{\nu_{\max}}\frac{\partial B_A}{\partial a_\nu}\Delta a_\nu .$$

The ratio and/or difference problem is linear in nature and is solved in a single iteration for the differences in charge distribution parameters Δa_ν and the incumbent error matrix. In order for either of these procedures (the absolute parameter fit or the parameter difference fit) to work properly, one must constrain the parameters such that the overall charge of the nucleus is maintained. This is done using the

technique of Lagrange multipliers. Failure to use this constraint can lead to a false minimum in χ^2 and an incorrect error matrix.

We have made fits to both the electron scattering data alone and to the combined electron scattering and muonic atom data. Satisfactory combined fits can be obtained, which we consider to be the best fits. However, if we use only the electron scattering data we find an rms radius consistently about 0.025 fm below the rms radius obtained from the combined fits. The generalized moment determined by the electron scattering data alone falls systematically below the measured values extracted from μ-mesic atom data. Table VI summarizes the resultant Fourier-Bessel coefficients for our best fits to the separate isotope data. For these fits we have assumed a cutoff radius $R=9$ fm and $\nu_{\max}=11$. Our value for R was chosen as intermediate between values of 8 and 12 fm used in similar analyses for ^{12}C and ^{208}Pb, respectively. Sensitivity of $\rho(r)$ to the choice of R is discussed in Ref. 7. The value of $\nu_{\max}$ was determined by the highest-q data (or pseudodata) used in the analysis: $\nu_{\max}=q_{\max}R/\pi$. One can see in Table VI that the last four Fourier-Bessel coefficients (8,9,10,11) are very poorly determined compared to the others, as one would expect from the upper limit nature of the pseudodata which largely determine these coefficients. Fits to the data using $\nu_{\max}>11$ were attempted, but failed to converge. The normalization factors N_k determined in the fits are given in Table VI. Table VI also shows our determination of the rms radii and generalized moments for each of the Cr isotopes under the specified conditions—(e,e) data alone and (e,e) plus μ-atom data. Uncertainties in these quantities were derived using the expression

$$\mathrm{var}f=\sum_{\mu\nu}\frac{\partial f}{\partial a_\mu}\frac{\partial f}{\partial a_\nu}\epsilon_{\mu\nu}\ ,$$

where $\epsilon_{\mu\nu}$ is the full variance-covariance or error matrix. It is evident that μ-mesic x-ray results are powerful complements to (e,e) results in improving the precision with which nuclear charge distributions are determined. For example, the normalization factor for the NIKHEF data is determined to about 0.25% with the Barrett moment and about 0.5% with just the electron data. In the Fourier-Bessel expansion method, addition of the muonic atom data improves only the determination of the first two coefficients a_1 and a_2, the statistical uncertainty decreasing by a factor of 4 for a_1 and 2 for a_2. These coefficients are determined by (or are equivalent to) electron scattering data at $q=0.3$ and 0.6 fm^{-1}, respectively.

The Fourier-Bessel coefficients for the difference charge distributions are summarized in Table VII.

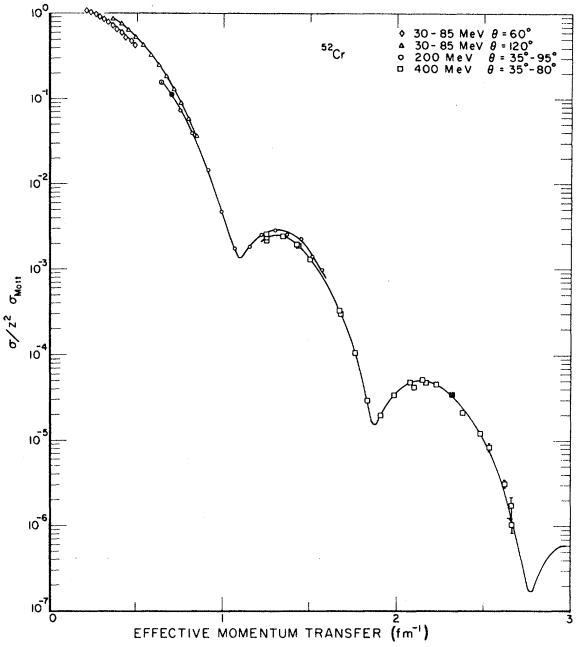

FIG. 1. Measured form factors ($\sigma/Z^2\sigma_{\mathrm{Mott}}$) for ^{52}Cr. The solid line is the best fit phase shift calculation from which the charge distribution was derived. Muonic data were used in determining this best fit. The symbols ■ and ● represent two independent measurements which fall within the symbol size, and correspondingly the symbol ⊙ represents three independent measurements.

The improved precision of both the electron scattering ratio data and the muonic atom difference data leads to an improved determination of the difference

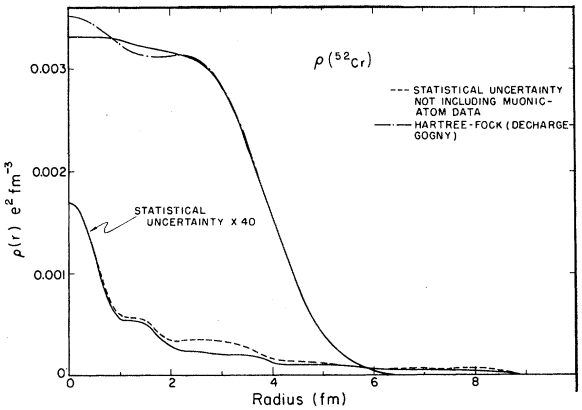

FIG. 2. Charge distribution for ^{52}Cr derived using the Fourier-Bessel expansion technique. The solid lines represent a combined analysis of (e,e') and muonic x-ray data, the dashed line indicating the uncertainty in $\rho(r)$ obtained without the muonic x-ray data. The Hartree-Fock calculation is shown by the dashed-dotted line.

TABLE VI. Summary $\rho(r)$ determination using Fourier-Bessel expansion. (a_ν) is a Fourier-Bessel coefficient derived from (e,e') and μ-x-ray data, a_ν^0 is Fourier-Bessel coeffient derived from (e,e') data alone. Similarly for the Barrett moments, B_k and B_k^0. The normalization factors $N_{1,2,3}$ correspond to normalizations for IKO, Saclay (200 MeV), Saclay (401.6 MeV), and Saclay (398.2 MeV), respectively. We use the following notation for uncertainties: 0.000(1)−2 corresponds to $0.000\times10^{-2}\pm0.001\times10^{-2}$.

	^{50}Cr				^{52}Cr				^{54}Cr			
ν	a_ν	(δa_ν)	a_ν^0	(δa_ν^0)	a_ν	(δa_ν)	a_ν^0	(δa_ν^0)	a_ν	(δa_ν)	a_ν^0	(δa_ν^0)
1	0.16321	(07)−2	0.16387	(26)−2	0.16367	(07)−2	0.16411	(27)−2	0.16249	(07)−2	0.16268	(25)−2
2	0.25757	(46)−2	0.25927	(80)−2	0.26028	(50)−2	0.26153	(92)−2	0.25124	(44)−2	0.25173	(78)−2
3	0.2856	(80)−3	0.2741	(92)−3	0.2603	(81)−3	0.2531	(92)−3	0.1910	(75)−3	0.1876	(87)−3
4	−0.1257	(13)−2	−0.1255	(13)−2	−0.1370	(12)−2	−0.1371	(13)−2	−0.1280	(12)−2	−0.1280	(12)−2
5	−0.4114	(97)−3	−0.420	(10)−3	−0.4436	(79)−3	−0.4481	(84)−3	−0.3806	(84)−3	−0.3831	(88)−3
6	0.3664	(65)−3	0.3695	(67)−3	0.4383	(65)−3	0.4415	(68)−3	0.3885	(61)−3	0.3897	(63)−3
7	0.2854	(81)−3	0.2846	(80)−3	0.3561	(67)−3	0.3549	(68)−3	0.2524	(62)−3	0.2522	(63)−3
8	−0.39	(33)−4	0.2	(3.5)−5	−0.10	(16)−4	−0.1	(1.7)−5	−0.65	(20)−4	−0.61	(21)−4
9	−0.104	(30)−3	−0.99	(31)−4	−0.85	(23)−4	−0.87	(22)−4	−0.32	(27)−4	−0.41	(27)−4
10	−0.64	(15)−4	−0.65	(15)−4	−0.50	(13)−4	−0.51	(12)−4	0.32	(11)−4	−0.34	(11)−4
11	−0.307	(94)−4	−0.349	(84)−4	−0.236	(76)−4	−0.262	(70)−4	−0.145	(57)−4	−0.135	(58)−4
N_1	1.0000	(23)	0.9902	(44)	1.0000	(26)	0.9932	(49)	1.0000	(23)	0.9971	(43)
N_2	1.0000	(96)	0.988	(11)	1.0000	(88)	0.990	(11)	1.0000	(94)	0.996	(11)
N_3	1.000	(30)	0.990	(30)	1.000	(23)	0.990	(24)	1.000	(26)	0.996	(27)
N_4	1.000	(24)	0.993	(25)	1.000	(22)	0.992	(22)	1.000	(23)	0.997	(23)
χ^2/n	47/79		41/78		88/86		86/85		77/82		76/81	
rms (fm)	3.6625	(38)	3.6284	(134)	3.6434	(33)	3.6217	(138)	3.6890	(37)	3.6793	(125)
B_k (fm^k)	11.685	(22)	11.517	(66)	11.578	(16)	11.469	(68)	11.846	(18)	11.798	(61)
B_k^0 (fm^k)	11.698	(19)			11.584	(17)			11.850	(19)		

TABLE VII. Summary—$\Delta\rho(r)$ determination using Fourier-Bessel expansion. Δa_ν is Fourier-Bessel coefficient derived from (e,e') and μ-x-ray data, Δa_ν^0 is Fourier-Bessel coefficient derived from (e,e') data alone. Similarly for the difference Barrett moments. The normalization factors $N_{1,2,3,4}$ correspond to normalizations for the ratio data for IKO, Saclay (200 MeV), Saclay (401.6 MeV), and Saclay (398.2 MeV), respectively. We use the following notation for uncertainties: $0.000(1)-2$ corresponds to $0.000\times10^{-2}\pm0.001\times10^{-2}$.

	^{52}Cr-^{50}Cr				^{54}Cr-^{52}Cr				^{54}Cr-^{50}Cr			
ν	Δa_ν	(δa_ν)	Δa_ν^0	(δa_ν^0)	Δa_ν	(δa_ν)	Δa_ν^0	(δa_ν^0)	Δa_ν	(δa_ν)	Δa_ν^0	(δa_ν^0)
1	0.503	(15)−5	0.41	(15)−5	−0.1176	(14)−4	−0.137	(22)−4	−0.684	(15)−5	−0.87	(15)−5
2	0.291	(39)−4	0.271	(65)−4	−0.893	(33)−4	−0.936	(60)−4	−0.632	(22)−4	−0.671	(39)−4
3	−0.33	(10)−4	−0.32	(12)−4	−0.655	(81)−4	−0.610	(96)−4	−0.948	(81)−4	−0.920	(84)−4
4	−0.114	(19)−3	−0.115	(19)−3	0.92	(15)−4	0.91	(15)−4	−0.18	(17)−4	−0.22	(17)−4
5	−0.22	(16)−4	−0.20	(16)−4	0.62	(10)−4	0.65	(11)−4	0.38	(13)−4	0.41	(13)−4
6	0.77	(11)−4	0.77	(10)−4	−0.481	(79)−4	−0.494	(80)−4	0.233	(91)−4	0.220	(91)−4
7	0.69	(14)−4	0.70	(14)−4	−0.898	(66)−4	−0.886	(67)−4	−0.240	(86)−4	−0.220	(87)−4
8	−0.30	(35)−4	−0.35	(38)−4	−0.30	(13)−4	−0.36	(15)−4	−0.4	(2.3)−5	−0.14	(24)−4
N_1	0.9992	(16)	1.0005	(37)	1.0002	(16)	1.0028	(34)	1.0002	(10)	1.0027	(22)
N_2	1.002	(13)	1.003	(13)	1.000	(11)	1.002	(11)	1.004	(11)	1.005	(11)
N_3	0.973	(47)	0.974	(47)	0.995	(30)	0.997	(30)	0.996	(40)	0.995	(40)
N_4	1.010	(38)	1.011	(38)	1.008	(27)	1.010	(27)	0.997	(34)	0.998	(34)
χ^2/n	42/60		42/59		75/62		74/61		35/60		35/59	
Δrms (fm)	−0.0199	(9)	−0.015	(13)	0.0451	(8)	0.055	(11)	0.0246	(8)	0.0343	(80)
ΔB_k (fm^k)	−0.1131	(29)	−0.089	(64)	0.2658	(29)	0.315	(56)	0.1524	(33)	0.200	(39)
ΔB_k^0 (fm^k)	−0.1138	(29)			0.2658	(29)			0.1520	(33)		

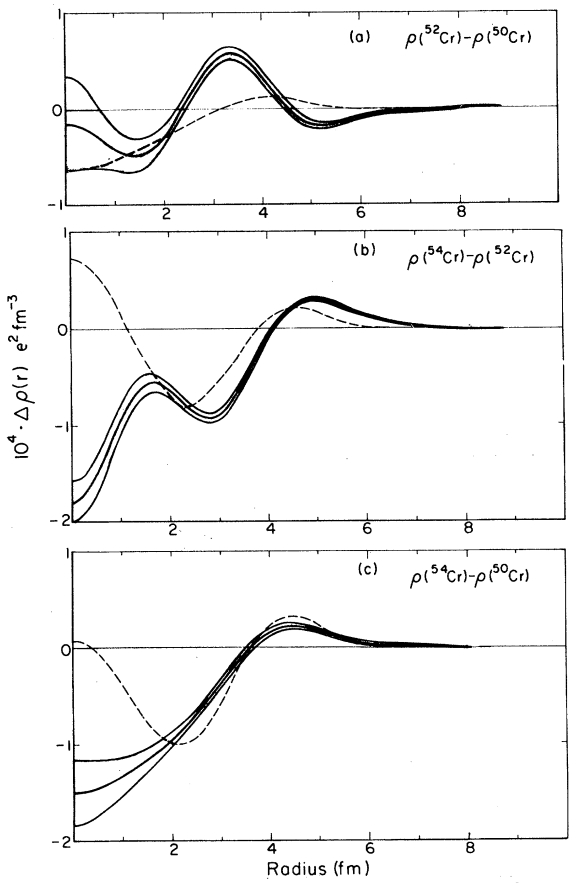

FIG. 3. The difference charge distributions for (a) $^{52-50}$Cr, (b) $^{54-52}$Cr, and (c) $^{54-50}$Cr derived using the Fourier-Bessel expansion technique. The analysis includes both (e,e') and muonic atom data. The Hartree-Fock calculations of the difference charge distributions are indicated by dashed lines.

in coefficients. As with the data for each separate isotope, the difference coefficients Δa_1 and Δa_2 are the only coefficients which show an improved determination through the addition of the muonic data, in this case by about a factor of 10 and 2, respectively. In Table VII we also summarize our results for the differences in rms radii and generalized moments for the isotope pairs considered.

Figure 1 shows the measured form factors for ^{52}Cr and the corresponding best fit. Figure 2 shows our resultant charge distribution for ^{52}Cr, and Fig. 3 shows the difference charge distributions: 52−50, 54−52, and 54−50. In obtaining difference distributions data we did not employ pseudodata; however, we did constrain the coefficients determined largely by the pseudodata $(a_{9,10,11})$ to be consistent with results of the fit to the separate isotope data. The uncertainty envelopes shown in Figs. 2 and 3 were computed using the full derived error matrix. These error bands do not include separate estimates made for systematic effects; i.e., such as folding in differences between best fit $\rho(r)$ using nominal systematic variables and best fit $\rho(r)$ using the same set of systematic variables except for one variable set to its extreme possible value. By experience the largest of these differences relates to overall normalization effects such as target thickness or detection efficiency. Since we did not experimentally determine this overall normalization factor, we cannot make such variations. Our experience with other data suggests that uncertainties given here (which neglect such variations) might be underestimated by as much as a factor of 2. We also should point out that the error bands indicated in Figs. 2 and 3 must be interpreted as single-point distribution functions, and should in

TABLE VIII. Summary rms radii determination. All results in fm. FB represents a Fourier-Bessel expansion result, while $2pF$ represents a two-parameter Fermi model fit to the data. We use the following notation for uncertainties: 0.000(1)−2 corresponds to $0.000\times10^{-2}\pm0.001\times10^{-2}$.

Data, analysis, or theory	^{50}Cr	^{52}Cr	^{54}Cr
rms [FB, (e,e')+muonic atom]	3.662(4)	3.643(3)	3.689(4)
rms [FB, (e,e')]	3.628(13)	3.622(14)	3.679(12)
rms [$2pF$, IKO (e,e')]	3.638(13)	3.613(17)	3.673(14)
rms (DDHFB[a])	3.602	3.603	3.625
	$^{52-50}$Cr	$^{54-52}$Cr	$^{54-50}$Cr
Δrms [FB, (e,e')+muonic atom]	−0.020(1)	0.045(1)	0.025(1)
Δrms [FB, (e,e')]	−0.015(13)	0.055(11)	0.034(8)
Δrms [$2pF$, IKO (e,e')]	−0.037(11)	0.065(9)	0.033(6)
Δrms [Shevchenko (e,e') Ref. 12]	−0.028(12)		0.068(12)
Δrms (DDHFB[a])	0.002	0.002	0.024

[a]Results of calculation by Dechargé and Gogny performed using the formalism presented in Ref. 3.

no way be interpreted as envelopes of all possible charge distribution profiles.

Table VIII summarizes the resultant rms radii and radii differences obtained by the present authors, by Lapikás[11] using a two-parameter Fermi model with only the NIKHEF data normalized to the ^{12}C measurements of NIKHEF, and results of measurements by Shevchenko *et al.*[12]

Our charge distributions have been compared with Hartree-Fock-Bogolyubov calculations done by Dechargé and Gogny.[3] These are shown in Figs. 2 and 3. For $r \leq 3$ fm there is considerably more oscillatory structure in the theoretical distribution for ^{52}Cr than indicated by the experimental charge distribution; cf. Fig. 2. Furthermore, the differences in the charge distributions for the different isotope pairs are not very well given by theory (cf. Fig. 3), especially for $r \leq 2$ fm. These failures of theory can possibly be attributed to shortcomings in the theory associated with deformations. The calculations were done using a spherical rather than a deformed basis, and nuclei in this region of atomic weight are thought to be relatively soft to deformation. The correct Hartree-Fock ground state should represent an integration over a wide distribution of different deformations. It therefore appears that more refined calculations are called for in order to understand the present resultant charge distributions on a microscopic shell model level.

IV. RESULTS—INELASTIC SCATTERING

The scope of the present inelastic studies includes measurement and analysis of form factors for 2^+, 4^+, and 6^+ states below an excitation energy (ω) of 4 MeV in each of the three isotopes. All measurements of the inelastic scattering form factors were made relative to the elastic scattering form factor for the appropriate target. The relative measurements were normalized using best fit elastic scattering cross sections for the various isotopes, taking target composition into account. The first approximation theoretical interpretation of the present data is in terms of the $f_{7/2}$ seniority coupling scheme, in which the low lying level structure is formed by breaking a coupled pair of $f_{7/2}$ protons and recoupling them to form 2^+, 4^+, and 6^+ states. Because of the nature of the pairing force the 0^+ (ground state), 2^+, 4^+, and 6^+ states are separated in energy by roughly equal amounts (Δ): $0^+(\omega=0)$, $2^+(\omega=\Delta)$, $4^+(\omega=2\Delta)$, and $6^+(\omega=3\Delta)$. In reality the known level schemes for the Cr isotopes are much more complicated than theory would predict (see Fig. 4). In particular, there are more 2^+ and 4^+ states than in the simple seniority scheme. In each of the isotopes studied here, there are two strongly

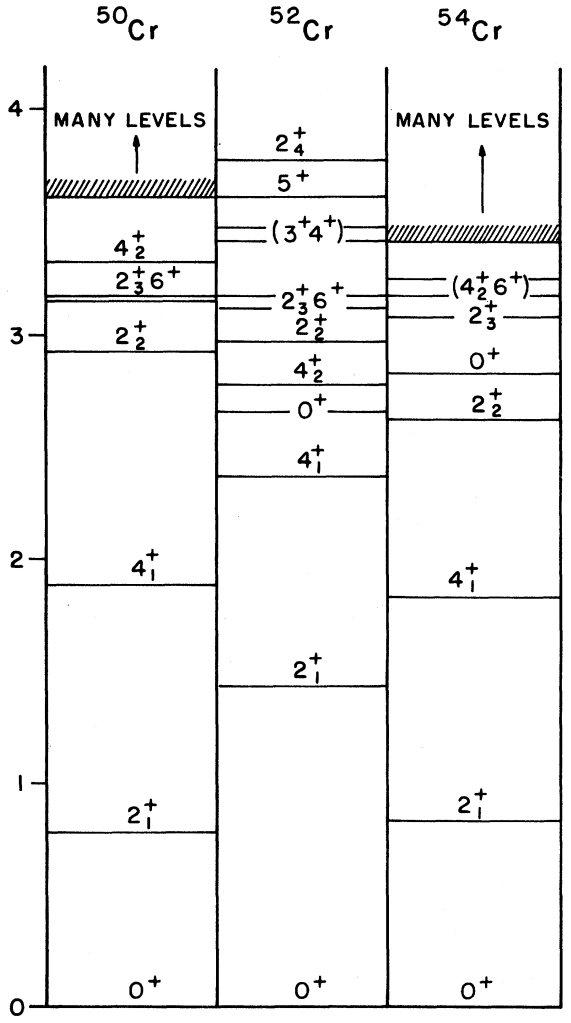

FIG. 4. Previously known level schemes for $^{50,52,54}Cr$. The excitation energies given on the left are in MeV.

excited 4^+ states. It has been suggested[13] that these two states arise because of seniority mixing, i.e., seniority 2 and 4. For the electromagnetic one body operator it is not possible to have transitions between the seniority 0 ground state and a seniority 4 excited state. What we see in our work are just the seniority 2 components of the excited states. The multiplicity of 2^+ states which we observe probably reflects similar mixing; however, in the case of 2^+ states, the first excited state has significantly more transition strength than any of the other 2^+ states. The presence of strongly excited 2^+, 4^+, and 6^+ states at roughly the spacing given by the seniority scheme, in each of the isotopes studied, indicates that the seniority scheme is reasonable, but is modified significantly by other shell model configurations and by coupling of these shells model states to

TABLE IX. 2_1^+ state—Tassie model parameters.

Isotope	$c_{tr}/c_{elastic}$	$c_{elastic}$ (fm)	$z_{tr}/z_{elastic}$	$z_{elastic}$ (fm)	$w_{tr}/w_{elastic}$	$w_{elastic}$	$\mathscr{B}/\mathscr{A}$	Q (fm^{-1})	$B(E2)$ e^2fm^4
^{50}Cr	0.9086	3.5741	0.9106	2.2762	3.575	0.1968	−0.1135	2.319	933 1020±30[a]
^{52}Cr	0.9159	3.6070	0.9211	2.2256	1.639	0.2449	−0.1027	2.634	632 660±30[a]
^{54}Cr	0.9744	3.5187	0.9282	2.2878	2.364	0.2898	−0.2793	2.168	949 850±30[a]

[a]Coulomb excitation measurements—Towsley *et al.* (Ref. 4).

core excitations. In the present work we examine the questions of configuration mixing and core polarization as they impact the radiative strength and q dependence of transitions to low-lying states. One should understand clearly that the calculated transition charges used in the present analysis were taken to be the same in ^{50,54}Cr as in ^{52}Cr. No attempt was made theoretically to include neutron contributions to these transitions, so that wave function does not have a proper isospin.

We have attempted to fit all data within the context of the shell model, using a DWBA phase shift code to generate theoretical cross sections from shell model transition charges. For the first 2^+ states (2_1^+) the simple shell model $f_{7/2}\rightarrow f_{7/2}$ transition is not adequate to describe the data. For these states we found that the Tassie model had sufficient freedom in form to fit the present data, provided a term was added to the transition charge density to fit the highest q data. Specifically we added a term

$$\Delta\rho(r)\sim j_2(Qr),\quad Q\approx q_{\max}\ ,$$

to the Tassie model transition charge (see below). We interpret the near adequacy of the Tassie model as a reflection of the collective nature of these states. Table IX gives resultant Tassie model parameters re-

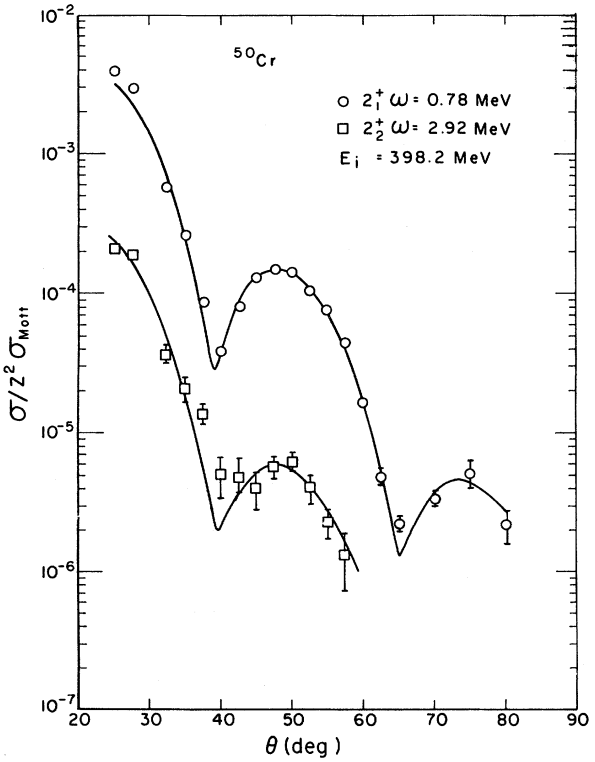

FIG. 5. Form factors for the ^{50}Cr 2_1^+ and 2_2^+ states. The solid curves are fits to the angular distributions using the Tassie model (2_1^+) or shell model (2_1^+). (See text.)

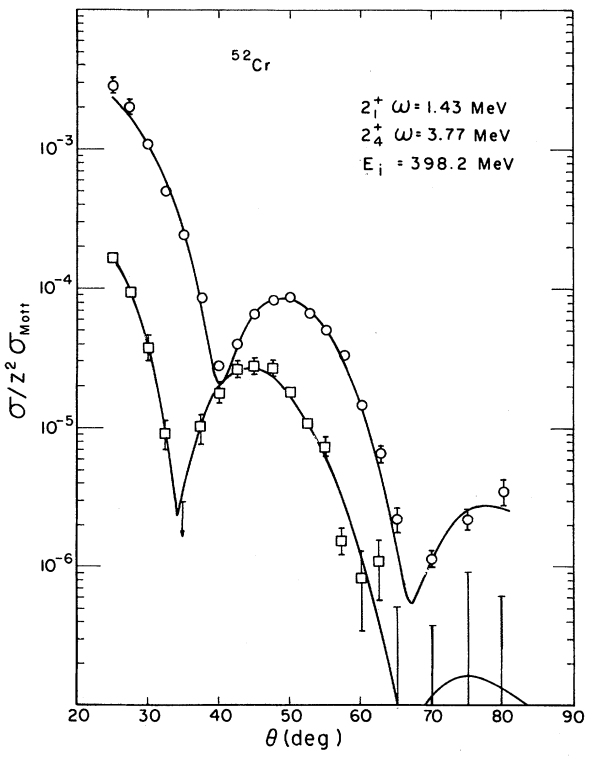

FIG. 6. Form factors for the ^{52}Cr 2_1^+ and 2_4^+ states. The solid curves are fits to the angular distribution using the Tassie model (2_1^+) or shell model (2_4^+). (See text.)

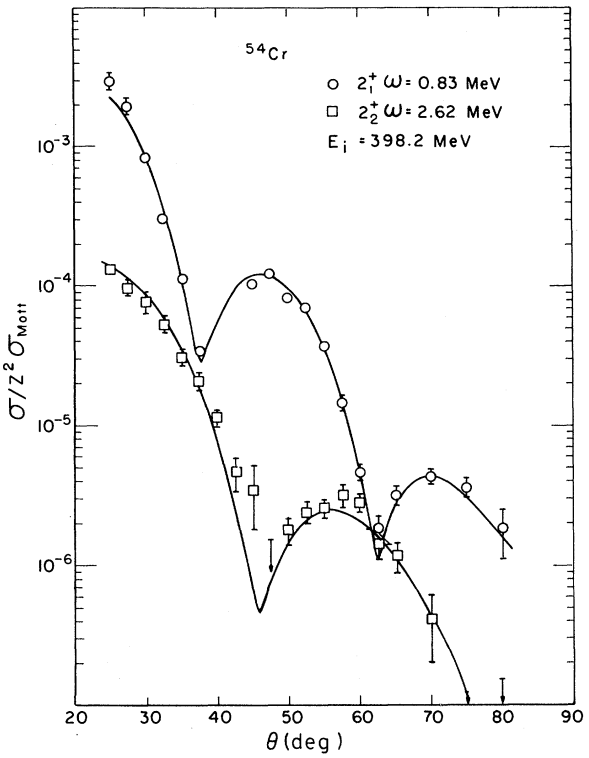

FIG. 7. Form factors for the ^{54}Cr 2_1^+ and 2_2^+ states. The solid curves are fits to the angular distribution using the Tassie model (2_1^+) or shell model (2_2^+). (See text.)

quired to fit the 2_1^+ state data, where the form of the Tassie model is

$$\rho^{(r)}_{\text{transition}} = \mathscr{A} r \left[\frac{d\rho_0(r)}{dr} \right]_{c=c_{\text{tr}},\, z=z_{\text{tr}},\, w=w_{\text{tr}}} + \mathscr{B} j_2(Qr) ,$$

where

$$\rho_0(r) = \left[1 + w \left(\frac{r}{c} \right)^2 \right] \Big/ [1+\exp((r^2-c^2)/z^2)] .$$

Also given in Table IX are our values for the $B(E2)$'s. The corresponding fits to these data are shown in Figs. 5–7. Given the lack of low-q data we consider the agreement of the present $B(E2)$ values with other measurements[4] to be reasonably good. However, because of the lack of this low-q data we hesitate to give uncertainties for the $B(E2)$'s. The effective charges (bare proton plus core polarization charge) necessary to bring the shell model prediction into agreement with our measured $B(E2)$ values are 2.66e, 2.18e, and 2.68e for the 2_1^+ states in ^{50}Cr, ^{52}Cr, and ^{54}Cr, respectively. In obtaining these values of e_{eff} we have assumed an oscillator parameter[14] $b=1.90$ fm. Clearly core polarization is very important. The appreciably smaller value of e_{eff} for ^{52}Cr suggests that the neutron shell closure at $N=28$ significantly reduces the $E2$ core polarizability.

The transitions to the higher excitation energy 2^+ states as well as the 4^+ and 6^+ states have been analyzed using harmonic oscillator shell model transition charges. In order to make a comparison between experimental and theoretical cross sections it is first necessary to fold in the effects of finite proton size and center-of-mass motion. This is done by multiplying theoretical shell model form factors by the product of the proton form factor $f_p(q)$ and the harmonic oscillator recoil factor f_R:

$$f_p = 1/(1+q^2 a_p^2/12)^2$$

and

$$f_R = \exp(q^2 b^2/4A) ,$$

where $a_p=0.84$ fm, b is the oscillator parameter, and A is the atomic mass. The shell model transition charge for $f_{7/2} \rightarrow f_{7/2}$ transitions ($\equiv ff$) in the seniority scheme is

$$\rho_{ff}(0^+ \rightarrow L^+) = a_L^{ff} b_f^{-9} r^6 \exp -(r/b_f)^2 ,$$

where

$$a_2^{ff} = -32/(21\sqrt{21}\pi) ,$$

$$a_4^{ff} = 64\sqrt{3}/(35\sqrt{77}) ,$$

and

$$a_6^{ff} = 64/(63\sqrt{11}\pi) .$$

For transition out of the $f_{7/2}$ shell to the $2p_{3/2}$ shell, the transition charge becomes

$$\rho_{fp}(0^+ \rightarrow L^+) = a_L^{fp} b_f^{-9/2} b_p^{-5/2} r^4 (1-(\tfrac{2}{5}) r^2/b_p^2) \exp(-(b_p^{-2}+b_f^{-2}) r^2/2) ,$$

where

$$a_2^{fp} = 8\sqrt{2}/(7\pi) ,$$

$$a_4^{fp} = -8\sqrt{10}/(21) ,$$

and $a_6^{fp} \equiv 0$ (not allowed). We have separated out the oscillator parameter for different orbitals (b_p and b_f) as an additional degree of freedom for fitting the experimental data. We have used the fact that the $0^+ \rightarrow 6^+$ transition occurs predominantly within the f shell to fit the f-shell oscillator parameter. Data for the $0^+ \rightarrow 6_1^+$ transition in ^{52}Cr were fit with b_f free and with the overall normalization free. Data for the $0^+ \rightarrow 6_1^+$ transition in the other isotopes were

TABLE X. 6^+ state transition charge parameters.

		b_f (fm)	$B(E6)$ $e^2\text{fm}^{12}$	e_{eff}
^{50}Cr	6_1^+	1.90	0.44×10^7	$0.49e$
^{52}Cr	6_1^+	1.90	0.143×10^8	$0.89e$
^{54}Cr	6_1^+	1.90	0.95×10^7	$0.73e$
	6_2^+	2.22	0.73×10^8	$1.71e$

not as precise as for the ^{52}Cr data, so b_f for ^{50,54}Cr was taken from ^{52}Cr and the normalization was made for the highest-q data where contributions from the unresolved 2^+ and 4^+ states were expected to be negligible. The data for the lowest excitation energy 6^+ states in ^{50,54}Cr were reasonably well described using the b_f from ^{52}Cr. In ^{54}Cr we have found what appears to be a second low excitation energy 6^+ state. Table X gives $B(E6)$ values, b_f, and effective charges for the $0^+ \rightarrow 6_1^+$ transitions in each isotope and for the possible $0^+ \rightarrow 6_2^+$ transitions in ^{54}Cr. The present data and our fits to these data are shown in Figs. 8–10. With the exception of the ^{54}Cr $0^+ \rightarrow 6_2^+$ transition, all the effective charges are less than the proton charge. These effective charges change substantially in going from ^{50}Cr to ^{54}Cr. One might expect that for ^{52}Cr, with a closed neutron shell, the effective charge measured should reflect the proton effective charge only. Sagawa[15] recently performed a core polarization calculation for $f_{7/2}$ shell 6^+ transitions and found little additional transition charge coming from core polarization: $\delta e_p = -0.06e$. Our result for ^{52}Cr is roughly consistent with this calculation, giving δe_p due to core polarization of $-0.11e$ (not considering neutrons at all). For the other isotopes studied, it appears that neutrons play an important role, decreasing the effective charge required to fit the 6_1^+ state data from $0.89e$ in ^{52}Cr to $0.49e$ and $0.73e$ for ^{50}Cr and ^{54}Cr, respectively.

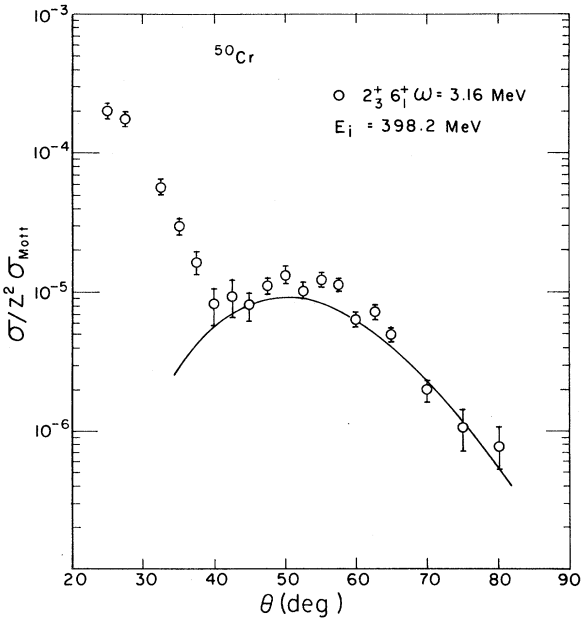

FIG. 8. Form factors for the ^{50}Cr unresolved 2_3^+ and 6_1^+ states. The solid curve is a shell model calculation with an oscillator parameter taken from a fit to the 6_1^+ state in ^{52}Cr. (See text.)

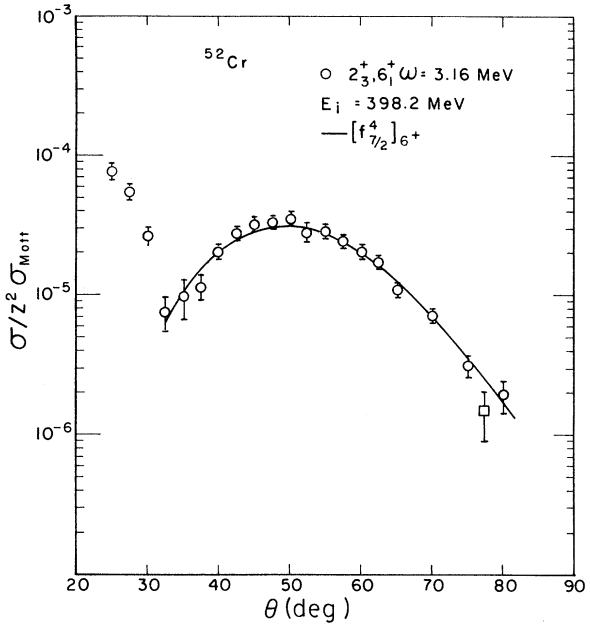

FIG. 9. Form factors for the ^{52}Cr unresolved 2_3^+ and 6_1^+ states. The solid curve is a shell model calculation for the 6_1^+ state in which the oscillator parameter b_f was adjusted to fit to these data. (See text.)

Our result for the effective charge of the 3.62 MeV 6_2^+ state in ^{54}Cr is greater than the ^{52}Cr 6_1^+ state effective charge. We do not know how to intepret this for lack of data on the higher excitation energy 6^+ states in ^{50,52}Cr. In order to check the multipolarity assignment we have also attempted to fit the data for the 3.62 MeV state in ^{54}Cr assuming it is a 5^- state rather than a 6^+ state. The two fits, 5^- and 6^+, are both shown in Fig. 10. We cannot tell which assignment is correct based on our data alone. The absence of a 5^- state in the literature and any other low lying negative parity states in the isotopes studied here makes us favor the 6^+ assignment. For the sake of completeness we have fit the 3.62 MeV state using the shell model transition charge for a $(1f_{7/2} \rightarrow 1g_{9/2})$ transition, and obtain a

$$B(E5) = 0.325 \times 10^6 e^2 \text{ fm}^{10}$$

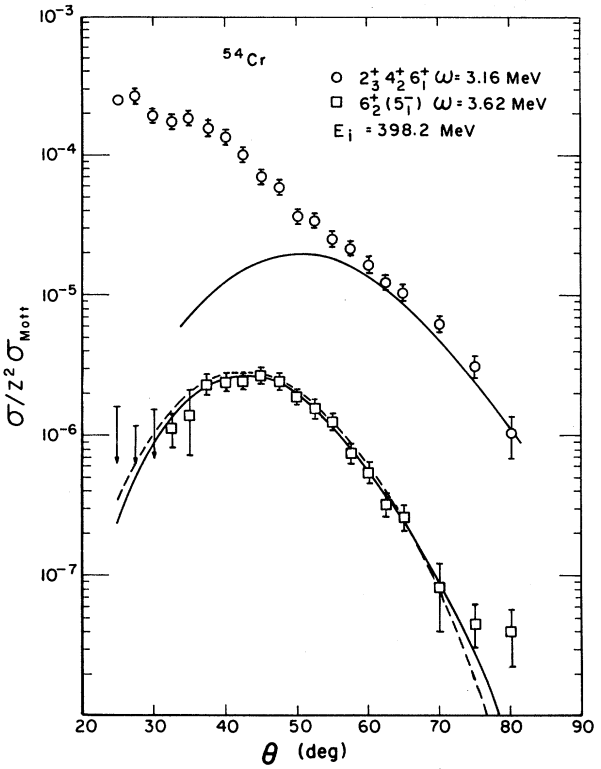

FIG. 10. Form factors for the ^{54}Cr unresolved 2_3^+, 4_2^+, and 6_1^+ states and for the ^{54}Cr 6_2^+ (or possibly 5_1^-) state. The solid lines are shell model calculations for the $6_{1,2}^+$ states, and the dashed curve is a shell model calculation assuming a 5^- transition. (See text.)

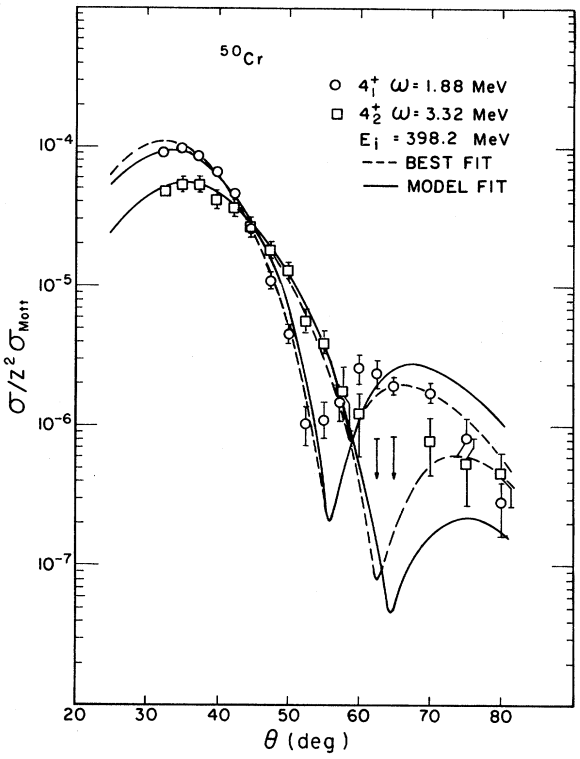

FIG. 11. Form factors for the ^{50}Cr 4_1^+ and 4_2^+ states. The solid curves are shell model calculations in which the oscillator parameters for the 4_1^+ and 4_2^+ states were chosen to be the same in the f shell, and in the p shell; i.e., $b_f(4_1^+)=b_f(4_2^+)$ and $b_p(4_1^+)=b_p(4_2^+)$. The dashed curves differ from the solid curves in that the p-shell oscillator parameter was allowed to vary independently for the 4_1^+ and 4_2^+ states. (See text.)

using an oscillator length parameter $b_f=b_g=1.83$ fm. Note that for a 6^+ transition the oscillator length parameter $b_f=2.23$ fm. As became apparent from fitting the 4^+ state data, these rather large deviations of b_f from "reasonable" values of b (1.9–2.0 fm) are not totally inconsistent with variations in model parameters required to fit 2^+ and 4^+ state data in the other isotopes of Cr. Our preference for the 6^+ assignment of the ^{54}Cr 3.62 MeV state is therefore only a rather weak preference.

Analysis of the 4^+ state data with the shell model transition charge is not as straightforward as analysis of the 6^+ state data. There are two closely spaced states with roughly equal transition strength, not one state as the simple seniority scheme would predict, in each isotope, and these states have different transition charges as evidenced by differences in the form factors. (See Figs. 11–13.) We have attempted to fit these data with a normalized linear combination of $(1f\rightarrow 1f)$ and $(1f\rightarrow 2p)$ transition amplitudes, using the same oscillator parameters for both 4^+ states. We begin by taking the $1f$-shell oscillator parameter b_f from the 6_1^+ state data (see Table X) and allowed the $2p$ shell oscillator parameter b_p to be free, along with the transition charge for each state. Fitting first the 4_1^+ and 4_2^+ state data for ^{52}Cr we find effective charges of $1.32e$ and $0.93e$, respectively, with normalized transition amplitudes $(1f\rightarrow 1f,\ 1f\rightarrow 2p)$ of (0.71, 0.71) and (0.87, 0.49), respectively, and with $b_p=1.94$ fm. The fact that we can achieve a reasonably good fit to these data (Fig. 12) using simple configuration mixing may be fortuitous, because the effective charges for the two transitions are different. One would expect that since we have chosen the same basis states to describe the two 4^+ states, the effective charges (e_{eff}) as well should be the same and the two wave functions orthogonal. If the 4_1^+ and 4_2^+ state wave functions were orthogonal then the above transition amplitudes, let us call them $(\alpha_1,\ \beta_1)$ and $(\alpha_2,\ \beta_2)$, should satisfy the relation $\alpha_1\alpha_2+\beta_1\beta_2=0$, yet clearly they do not. Allowing possible seniority mixing, orthogonality and normalization relations must be modified. Electron scattering does not ac-

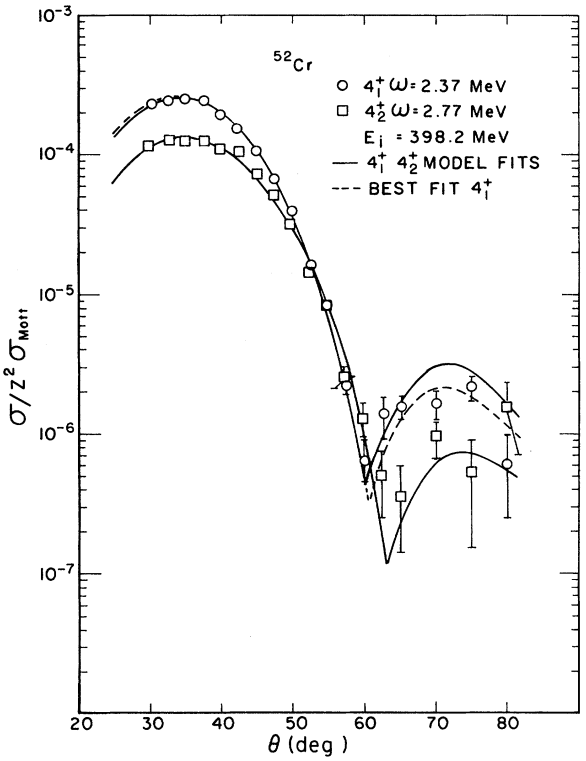

FIG. 12. Form factors for the ^{52}Cr 4_1^+ and 4_2^+ states. The solid curves are shell model calculations in which the oscillator parameters for the 4_1^+ and 4_2^+ states were chosen to be the same, i.e., $b_f(4_1^+)=b_f(4_2^+)$ and $b_p(4_1^+)=b_p(4_2^+)$. The dashed curve differs from the solid curves in that the p-shell oscillator parameter was allowed to vary independently for the 4_1^+ and 4_2^+ states. The f-shell oscillator parameter is the same as obtained in the 6_1^+ state fit. (See text.)

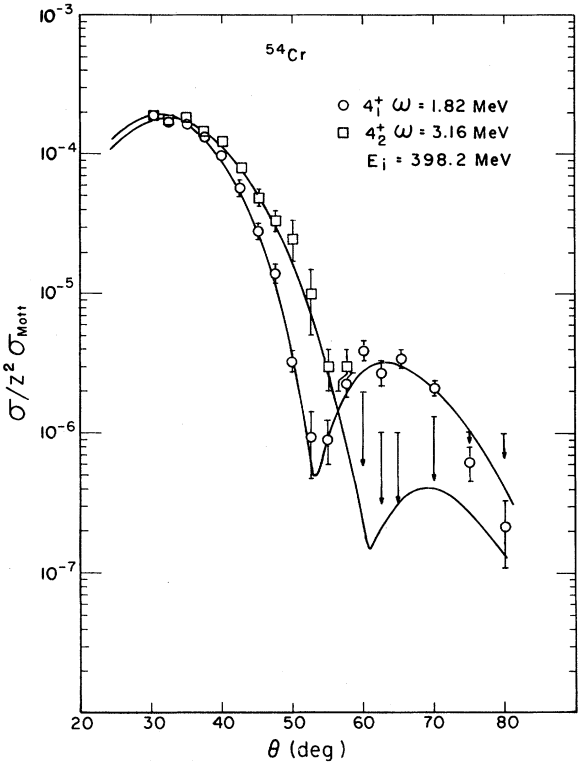

FIG. 13. Form factors for the ^{54}Cr 4_1^+ and 4_2^+ states. The solid curves are shell model calculations in which the oscillator parameters for the 4_1^+ and 4_2^+ states were chosen to be the same in the f shell, and in the p shell; i.e., $b_f(4_1^+)=b_f(4_2^+)$ and $b_p(4_1^+)=b_p(4_2^+)$. (See text.)

cess the seniority 4 amplitudes of the $4_{1,2}^+$ state wave functions. One can then construct a three-component wave function which includes seniority 4 amplitudes in the final state:

$$\psi(4_{1,2}^+)=\alpha_{1,2}\phi(1f_{7/2}{}^4,n=2)+\beta_{1,2}\phi(1f_{7/2}{}^3 2p_{3/2})+\gamma_{1,2}\phi(1f_{7/2}{}^4,n=4)\ ,$$

where the ϕ's are normalized shell model wave functions, n is the seniority quantum number, and the amplitudes $\alpha_{1,2}$, $\beta_{1,2}$, and $\gamma_{1,2}$ are normalized and satisfy the orthogonality condition. In order to retain our fit to the $4_{1,2}^+$ state data, we must scale the effective charge and transition amplitudes in such a way as to preserve the product; i.e.,

$$4_1^+:\ e_{\rm eff}(4_1^+)\times(0.71,0.71)\rightarrow\frac{e_{\rm eff}(4_1^+)}{f_1}\times(0.71f_1,0.71f_1)$$

and

$$4_2^+:\ e_{\rm eff}(4_2^+)\times(0.87,0.49)\rightarrow\frac{e_{\rm eff}(4_2^+)}{f_2}\times(0.87f_2,0.49f_2)\ .$$

The effective charges become $e_{\rm eff}(4_{1,2}^+)/f_{1,2}$, with $f_{1,2}\leq 1$, and the transition charge amplitudes for the $4_{1,2}^+$ state are reduced by the factors $f_{1,2}$. This latter reduction allows us to add a seniority $n=4$ component to the $4_{1,2}^+$ state wave functions with amplitudes $\pm(1-f_1{}^2)^{1/2}$ and $\pm(1-f_2{}^2)^{1/2}$, respectively.

TABLE XI. Model wave functions for $4^+_{1,2}$ states in ^{50,52,54}Cr.

		α	β	γ	b_f (fm)	b_p (fm)	e_{eff}	$B(E4)$ (e^2fm^8)	Comments
^{50}Cr	4^+_1	0.404	0.781 ±	0.476	1.88	1.99	1.07e	0.451×10^5	a,d Best fit, three-component model
		0.459	0.888		1.88	1.99	0.94e	0.451×10^5	b
		0.620	0.785		1.88	2.34	1.12e	0.666×10^5	c
	4^+_2	0.510	0.237 ∓	0.826	1.88	1.99	1.07e	0.192×10^5	a,d Best fit, three-component model
		0.907	0.421		1.88	1.99	0.60e	0.192×10^5	b
		0.683	0.730		1.88	1.79	0.59e	0.172×10^5	c
^{52}Cr	4^+_1	0.583	0.583 ±	0.565	1.90	1.94	1.60e	0.101×10^6	a,d Best fit, three-component model
		0.699	0.715		1.90	1.94	1.32e	0.101×10^6	b
		0.626	0.780		1.90	2.10	1.47e	0.116×10^6	c
		0.58		0.81					e
		0.583	0.360	0.728					f (theory)
	4^+_2	0.505	0.284 ∓	0.815	1.90	1.94	1.60e	0.482×10^5	a,d Best fit, three-component model
		0.874	0.485		1.90	1.94	0.93e	0.482×10^5	b
		0.81		−0.58					e
		0.748	0.346	0.566					f (theory)
^{54}Cr	4^+_1	0.488	0.570 ±	0.661	2.10	2.14	1.50e	0.167×10^6	a,d Best fit, three-component model
		0.650	0.760		2.10	2.14	1.13e	0.167×10^6	b
	4^+_2	0.725	0.150 ∓	0.672	2.10	2.14	1.50e	0.126×10^6	a,d Best fit, three-component model
		0.979	0.203		2.10	2.14	1.11e	0.126×10^6	b

[a]Fit uses same b_f and b_p for both 4^+_1 and 4^+_2 states of the present data.
[b]Two component model fit to present data, b_f and b_p the same for both 4^+_1 and 4^+_2.
[c]A best fit performed separately on the present 4^+_1 and 4^+_2 states; no regard to keeping b_f and b_p the same for the two states.
[d]Only the relative phase of the two γ components [$\gamma(4^+_1)$, $\gamma(4^+_2)$] is established as negative.
[e]Based on radiative decay of the 6^+_1 state to the $4^+_{1,2}$ states (Ref. 13).
[f]Only the magnitude of these amplitudes given in Ref. 16.

We then adjust f_1 and f_2, maintaining the normalization on $\psi(4_{1,2})$ until the orthogonality condition is also satisfied. For the ^{52}Cr data, using $f_1=0.825$ and $f_2=0.580$, we achieve a condition where the wave functions $\psi(4^+_{1,2})$ are orthogonal, normalized, and the effective charges required to yield the correct fits to the data for both states are the same: $e_{\text{eff}}=1.6e$. The coefficients $\alpha_{1,2}$, $\beta_{1,2}$, and $\gamma_{1,2}$ are given in Table XI. We give other results for such model wave functions based on either theory or radiative decay measurements. However, $2p_{3/2}$ configurations were not considered in deriving wave functions based on these latter measurements. The present results require such configurations. The wave functions resulting from the radiative decay measurements were obtained from the branching ratio for the decay of the 6^+_1 state to the $4^+_{1,2}$ states. According to the seniority coupling scheme, the 6^+_1 state has pure $n=2$ seniority and can decay by emission of $E2$ radiation only to 4^+ states with $n=2$ seniority. One can infer from the branching ratio that the seniority must be mixed in the two 4^+ states. Examining Table XI one can see that neither the two-component wave function amplitudes of Brown *et al.*[13] nor the three-component theory of Auerbach[16] is consistent with the present measurements. We feel that the disagreement between the (e,e') and γ-decay model amplitudes for ^{52}Cr may reflect seniority mixing in the 6^+ states, as well as in the 4^+ states.

The single most interesting aspect of the present $4^+_{1,2}$ data is the difference in shape of the two form factors. We can simulate this difference with linear combinations of the two transition charges ($1f\rightarrow1f$) and ($1f\rightarrow2p$), the latter containing a node. Owing to the presence of this node and to the relative phase of the two components, a minor change in the amplitudes will dramatically change the small-r transition charge density, hence the high-q form factor. In Fig. 10, we also show a fit to the 4^+_1 state in which b_p was allowed to vary, minimizing χ^2 for the 4^+_1 state fit, with no regard to χ^2 for the 4^+_2 state fit. Clearly, the fit to the high-q data can be improved by relaxing the model somewhat; however, this procedure destroys the synthesizing aspect of the model which made it interesting to begin with. For ^{50}Cr and ^{54}Cr, we have made similar two- and three-component fits to the combined 4^+_1 and 4^+_2 state data. Here, however, we have allowed b_f to be a free parameter, not fixing it to the 6^+_1 state value which was chosen more or less arbitrarily to be the same as the ^{52}Cr 6^+ state value. For ^{50}Cr the value

of b_f found to describe the 4^+ state data is essentially the same as that used to describe the 6_1^+ state data, 1.88 fm (^{50}Cr) vs 1.90 (^{52}Cr). For ^{54}Cr we found $b_f = 2.10$ fm from the 4^+ data. This value is to be compared with $b_f = 1.90$ fm used in describing the 6_1^+ state data, and $b_f = 2.10$ fm used in describing the 6_2^+ state data. The fits are shown in Figs. 9 and 11. Note that the ^{54}Cr 4_2^+ state data has been obtained by subtracting the 6_1^+ state fit from the unresolved 2_3^+-4_2^+-6_1^+ complex of states. Following the analysis used to generate ^{52}Cr model wave functions, we obtained effective charges and amplitudes for the multicomponent wave functions describing the $4_{1,2}^+$ states of ^{50}Cr and ^{54}Cr. These are also given in Table XI along with the ^{52}Cr results discussed earlier. In Table XI, we also give the two-component wave function amplitudes ($1f \rightarrow 1f$) and ($1f \rightarrow 2p$), and the effective charges, the oscillator parameters, and the reduced transition probabilities $B(EL)$ for the various 4^+ states which we studied. Included here are best fits (labeled *b*) where b_f and b_p were held to the same value for both the 4_1^+ and 4_2^+ states. In certain instances we relaxed the requirement that b_f and b_p be the same for both states in order to achieve a better fit. These fits are labeled "*c*" in Table XI. One should note the substantial differences in effective charges used to describe the $0^+ \rightarrow 4^+$ transition for the two- and three-component model wave functions.

In Table XII, we give results of our analysis of the other 2^+ states for which we have data. All of these states are weakly excited compared to the 2_1^+ states, and display form factors which differ significantly from the 2_1^+ state form factors. These data for the higher excitation energy 2^+ states are presented in Figs. 5–10. The 2_3^+ states in each isotope lay very close in excitation energy to the 6_1^+ states. Of these 2_3^+ states only those in ^{50}Cr and ^{52}Cr were seen, and it is only because of the great difference in q dependence of the unresolved 2^+ and 6^+ state form factors that we can even estimate the 2_3^+ state strengths. We have not attempted to fit these 2_3^+ state data with shell model transition charges simply because the data do not extend over a large enough q range. Instead we have scaled the 2_1^+ state form factors to fit the 2_3^+ data, and present rough $B(E2_3^+)$ values. We do not have sufficient data on several other 2^+ states which warrant a more detailed analysis—and 2_2^+ states in ^{50,54}Cr and the 2_4^+ state in ^{52}Cr. We have attempted to fit these data using the ($1f \rightarrow 1f$) and ($1f \rightarrow 2p$) shell model transition charges given earlier. Our fits to these data are shown in Figs. 5–7. The resultant model parameters are given in Table XII. The 2_2^+ state in ^{54}Cr was not seen in the present work, and the 2_3^+ state in ^{54}Cr was not resolvable from the 4_2 and 6_1^+ states.

As with the 2_1^+ state data and for lack of low-q data, we have not given uncertainties in the other measured $B(E2)$ values. Neither have we given uncertainties in $B(E4)$ or $B(E6)$ values. The strength of the present measurements lies not in determining reduced probabilities, but in sensitivity to detailed radial dependence in the transition charge density and wave functions.

V. DISCUSSION AND CONCLUSION

From the present elastic scattering data, which cover a momentum transfer range from 0.15 to 2.6 fm^{-1}, we have derived ground state charge distributions for ^{50,52,54}Cr. We have included μ-mesic x-ray data in this analysis and are able to find a satisfactory combined fit, although the electron data alone lead systematically to $\sim$0.025 fm smaller rms radii than obtained in the combined analysis. We have also obtained a determination of the difference charge distributions, again in combination with μ-

TABLE XII. $2_{2,3,4}^+$ state model parameters for ^{50,52,54}Cr.

		α	γ	b_f (fm)	b_p (fm)	e_{eff}	$B(E2)$ (e^2fm^4)	Comment
^{50}Cr	2_2^+	0.934	0.358	2.00	2.26	0.70	89	
	2_3^+	1		1.91		0.72		a
^{52}Cr	2_3^+	1		1.91		0.34	16	a
	2_4^+	0.715	0.699	1.90	2.37	2.37	112	
	$2_{3,4}^+$						15,107	b
^{54}Cr	2_2^+	0.865	0.502	1.73	2.59	1.06	26	c

[a]These $B(E2)$ values are rough estimates based on scaling to the 2_1^+ state data. In extracting e_{eff} we compared our $B(E2)$ to the shell model value for $B(E2)$ using the given value of b_f.
[b]This is result of J. E. P. de Bie, IKO, thesis , 1975 (unpublished).
[c]In order to fit these data we found it neccesary to free the form of the polynomial in $\rho_{fp} \propto (1-0.4r^2/b_p)$. Finally, we used $(1-0.44r^2/b_p)$.

mesic x-ray data. As far as we know from published data, the present work is one of the most precise comparisons of electron scattering and muon data, where (1) a strong overlap of momentum transfers exists (muon data corresponding to low $q \sim 0.3$–0.6 fm electron scattering data) and (2) an extended momentum transfer range exists for determining details of $\rho(r)$. For other nuclei[17] such comparisons have been made, but the low-q data have large uncertainties (2% or more). The present low-q data, even folding in the carbon reference cross sections, have uncertainties significantly below one percent. We note, however, that low Fourier-Bessel coefficients in the combined e fits are still largely determined by the muon data. This effect means that the normalization of the low-q electron data, being free, will be adjusted to fit the constraints imposed by the muon data. In order to improve comparison between electron and muon probes of the nuclear charge distribution, future work should concentrate on a precise determination of the electron data normalizations. Comparison of the present charge distributions with the Hartree-Fock-Bogolyubov calculations of Dechargé and Gogny using a spherical basis indicates that there are serious problems with theory in the region $r \lesssim 2$ fm. Improvements here may conceivably involve use of a deformed set of basis states.

Inelastic scattering results for the 2^+, 4^+, and 6^+ state have been obtained in the q range from 0.9 to 2.6 fm^{-1} and interpreted in terms of shell model transition charge densities. It is apparent that in order to describe the 2^+ and 4^+ state data, significant mixing of $1f_{7/2}$ and $2p_{3/2}$ configurations is required. Core polarization is also required to describe the strength of essentially all the states studied. In ^{52}Cr, where the $f_{7/2}$ neutron shell closes, we view the 6_1^+ state transition as predominantly a proton transition. The additional proton core polarization charge required to describe this transition is negative. The effect of adding or subtracting two neutrons from ^{52}Cr is to open up neutron degrees of freedom which can either enhance or reduce the 6_1^+ transition strength. The present 6_1^+ state data indicate that the latter is the case, which would naively indicate a negative core polarization charge for the valence neutron. The effective charge required in the $4_{1,2}^+$ state transitions, if we view these as simple seniority type shell model transitions, is between $1.1e$ and $1.6e$. For the highly collective 2_1^+ state transitions the effective charge exceeds $2e$. This multipole dependence of the core polarization charge has been interpreted by Horikawa *et al.*[18] using an analysis of the effective two-nucleon interaction which requires the triplet-odd state component of the residual interaction to be strongly attractive. Most effective interactions are either repulsive or zero in the triplet-odd state. Sagawa has shown that the observed multipole dependence of the proton core polarization charge can be explained using a density dependent residual interaction, removing the necessity for the attractive triplet-odd residual interaction. These same calculations also produce a relatively large positive polarization charge for neutrons. This is in contradiction to our present observation concerning the 6_1^+ state transition strength in ^{50}Cr and ^{54}Cr. Since there is a reduction in the strength of the 6_1^+ states in ^{50,54}Cr with respect to ^{52}Cr, we have some indication for a negative effective charge for neutrons. Clearly there is a need here for more detailed shell model calculations for these nuclei—including the effects of valence neutron, $1f$-$2p$ shell configuration mixing, and seniority mixing. It would be extremely useful to have more data on predominantly neutron transitions in order to investigate the neutron core polarization charge. As suggested by Horikawa *et al.*, the low-lying positive parity states in ^{42}Ca would be a good case to study since the proton d shell is closed for Ca. An investigation of the current part of these positive parity transitions by 180° electron scattering would also be valuable to test the adequacy of any shell model calculations for these states.

ACKNOWLEDGMENTS

We wish to thank Dr. Dechargé and Dr. Gogny for performing the Hartree-Fock-Bogolyubov calculations shown herein. Part of this work was sponsored by the Stichting voor Fundamenteel Onderzoek der Materie (FOM) which is financially supported by the Nederlandse Organisatie voor Zuiver Wetenschappelijk Onderzoek (ZWO).

---

*Permanent address: National Bureau of Standards, Washington, D. C. 20234.

[1] *Proceedings of the Topical Conference of the Structure of $1f_{7/2}$ Nuclei,* edited by R. A. Ricci (Editrice Compositori, Bologna, 1971).

[2] H. D. Wohlfahrt *et al.*, Phys. Rev. C 23, 533 (1981).

[3] J. Dechargé and D. Gogny, Phys. Rev. C 21, 1568 (1980).

[4] C. W. Towsley, D. Cline, and R. N. Horoshko, Nucl. Phys. A250, 381 (1975).

[5] P. Leconte *et al.*, Nucl. Instrum. Methods 169, 401 (1980).

[6] L. C. Cardman *et al.*, Phys. Lett. 91B, 203 (1980).

[7] B. Dreher *et al.*, Nucl. Phys. A235, 219 (1974).

[8] J. Heisenberg, private communication.

[9] J. Borysowicz and J. H. Hetherington, Phys. Rev. C 7,

2293 (1973).
[10]E. B. Shera *et al.*, Phys. Rev. C 14, 731 (1976).
[11]J. J. Lapikas, thesis, University of Amsterdam, 1976.
[12]N. G. Shevchenko *et al.*, Yad. Fiz. 28, 139 (1978).
[13]B. A. Brown, D. B. Fossan, J. M. McDonald, and K. A. Snover, Phys. Rev. C 9, 1033 (1974).
[14]We note that the $1f_{7/2}$ proton and neutron radial distributions have been obtained at Saclay by P. K. A. deWitt-Hubert *et al.* [Phys. Lett. 71B, 317 (1977)], and by S. K. Platchkov *et al.* [Phys. Rev. C 25, 2318 (1982)], both using backward-angle electron scattering. These results yield values for b_f of 1.88±0.02 fm (protons) and 1.89±0.02 fm (neutrons).
[15]H. Sagawa, Phys. Rev. C 19, 506 (1979).
[16]N. Auerbach, Phys. Lett. 24B, 260 (1967).
[17]J. L. Friar and J. W. Negele, Nucl. Phys. A212, 93 (1973).
[18]Y. Horikawa, T. Hoshino, and A. Arima, Phys. Lett. 63B, 134 (1976).